Magneto-inductive cable arrays: Estimation and reduction of crosstalk

R. R. A. Syms[a] and L. Solymar
Optical and Semiconductor Devices Group, EEE Department, Imperial College London, Exhibition Road, London SW7 2AZ, UK

(Received 12 October 2010; accepted 13 December 2010; published online 23 February 2011)

Magneto-inductive waveguides are linear periodic structures consisting of regular arrangements of *L-C* resonators coupled together by mutual inductances *M*. Magneto-inductive cable is a low-loss flexible variant, based on overlapping inductors and parallel plate capacitors formed by double-sided patterning of copper-clad polyimide. The properties of cable arrays formed from a set of parallel magneto-inductive lines are investigated. Numerical solutions are provided for typical arrangements. Analytic methods are introduced for estimating the coupling between elements in neighboring cables and the frequency dependence of cross-talk. Theoretical confirmation is provided by experimental results for cables operating at ≈100 MHz. Strategies for reducing cross-talk using alternative element designs that achieve low mutual inductance by cancellation of induced currents are explored. © *2011 American Institute of Physics*. [doi:10.1063/1.3549147]

I. INTRODUCTION

Magneto-inductive (MI) media are low-frequency metamaterials consisting of periodic arrays of magnetically coupled *L-C* resonators. Linear arrangements form simple waveguides and devices,[1–3] while 2D and 3D arrangements form bulk media that can exhibit a wide variety of phenomena including negative refraction.[4,5] The effects of radiation and interaction with electromagnetic waves have been explored.[6–8] Propagation losses have been reduced,[9] nonnearest neighbor interactions have been confirmed,[10] and biperiodic structures have been investigated.[11–13] Many applications have been proposed, including delay lines,[13] phase shifters,[14] couplers and splitters,[3,15,16] concentrators,[17,18] near-field lenses,[19–22] detectors for magnetic resonance imaging,[23,24] safe interconnects for internal MRI,[25] and data transfer channels.[26] Parametric amplification has been suggested as a method of reducing propagation loss[27] and has been demonstrated experimentally.[28,29] Planar magneto-inductive waveguides are derivatives of microstrip filters based on magnetically coupled resonators.[30,31] Similar phenomena have been suggested or observed in other magnetically coupled media, including split-ring[32–37] and 'Swiss roll'[38,39] arrays. At higher frequencies, the phenomena have been rechristened magnetization waves[40,41] and magnetic plasmons.[42]

Until recently, MI waveguides have suffered from several drawbacks. Fabrication of large numbers of carefully tuned discrete resonators has been tedious. Weak coupling has led to high propagation losses. Poor coupling to systems with resistive impedance has led to reflections at input and output, and local variations in resonant frequency or coupling have also given rise to reflections. Overall system performance has therefore been poor, and measurements of MI phenomena have often been masked by standing-wave effects.

A new type of MI waveguide material has been demonstrated recently that overcomes many of these difficulties. The waveguide is a flexible cable,[43] which uses double-sided patterning of copper-clad polyimide to form overlapping inductors and parallel plate capacitors, with the thin substrate as an interlayer dielectric. High component values allow operation at low (ca 100 MHz) frequencies, high mutual inductance allows low-loss propagation, and lithographic definition eliminates variations in line properties. Elements may be distorted significantly without changing mutual inductance, allowing propagation through bends with low reflection.[44] Finally, an effective broadband method of coupling to resistive systems has been developed, based on a modified resonant element.[45]

Magneto-inductive cables may be configured as a parallel array, to provide multiple signal channels or a coherent image-transfer system. However, given the weak confinement of the magnetic field, coupling between adjacent lines must occur. In fact, a cable array will act much like a coupled optical waveguide array, an arrangement well known to spread the power in a guide to its neighbors.[46–48] Cross-talk between cables may then arise, which is clearly a disadvantage if a set of lines is to be used to transmit different signals.

In this paper, we consider the likely effects and strategies to reduce cross-talk. Although a MI cable array is geometrically similar to a 2D metamaterial, this viewpoint is different from the conventional one, where transverse coupling effects are tolerated. In Sec. 2, the properties of MI waveguides and coupled systems are briefly reviewed. In Sec. 3, analytic formulae that can allow estimation of cross-talk between coupled lines are presented. In Sec. 4, magneto-inductive cables are introduced and a simple method for evaluating the different coupling coefficients in arrays is demonstrated. In Sec. 5, the modifications to the model required for cable arrays are described. In Sec. 6, experimental results are presented for thin-film cables operating at ≈100 MHz frequency. In Sec. 7, improved element designs

[a]Electronic mail: r.syms@imperial.ac.uk

with the capability of reducing cross-talk are discussed. Conclusions are presented in Sec. 8.

II. MAGNETO-INDUCTIVE WAVEGUIDES AND DIRECTIONALLY-COUPLED SYSTEMS

We begin with a brief review of MI waveguides and directionally coupled systems.

A. Magneto-inductive waveguides

Figure 1(a) shows a MI waveguide, which consists of a linear arrangement of *L-C* resonators coupled together by mutual inductances *M*. The period is *a*, and the current in the n^{th} element is I_n. In general, the inductors will contain additional resistance *R*, which will give rise to propagation losses; however, for simplicity, we shall ignore loss. At angular frequency ω, the current in each loop satisfies the recurrence relation[1,2]:

$$(1-\omega_0^2/\omega^2)I_n+(\kappa/2)(I_{n-1}+I_{n+1})=0. \tag{1}$$

Here $\omega_0=1/(LC)^{1/2}$ is the angular resonant frequency of each loop and $\kappa=2M/L$ is the longitudinal coupling coefficient. κ can be positive or negative, depending on the physical arrangement of the guide and, when positive, has a maximum possible value of 2.

The waveguide supports traveling current waves of the form $I_n=I_0\exp(-jnka)$, where *k* is the propagation constant, and substitution into Eq. (1) yields the dispersion relation:

$$1-\omega_0^2/\omega^2+\kappa\cos(ka)=0. \tag{2}$$

For every value of *ka*, the angular frequency may be found as $\omega/\omega_0=1/\sqrt{\{1+\kappa\cos(ka)\}}$. Equation 2 implies that a MI waveguide supports waves over a finite range of angular frequency, such that $1/\sqrt{(1+|\kappa|)}\le\omega/\omega_0\le 1/\sqrt{(1-|\kappa|)}$. For positive κ, the waves are of forward type and for negative κ of backward type. The characteristic impedance is $Z_0=j\omega M\exp(-jka)$, which has the real value $Z_{0M}=\omega_0 M$ at mid-band $(ka=\pi/2)$.[4]

B. Directionally-coupled magneto-inductive systems

When MI waveguides are combined in a planar array, there will be additional mutual inductance between adjacent lines. The simplest case is a two-line system, formed from a pair of identical guides arranged parallel to each other so that adjacent elements in different lines are coupled by mutual inductances M′ as shown in Fig. 1(b). This arrangement is well known to act as a directional coupler.[3,15,16] Assuming that the currents in the n^{th} elements of lines 1 and 2 are $I_{1,n}$ and $I_{2,n}$ respectively, the governing equations are[3]:

$$\begin{aligned}(1-\omega_0^2/\omega^2)I_{1,n}+(\kappa/2)(I_{1,n-1}+I_{1,n+1})+(\kappa'/2)I_{2,n}=0,\\ (1-\omega_0^2/\omega^2)I_{2,n}+(\kappa/2)(I_{2,n-1}+I_{2,n+1})+(\kappa'/2)I_{1,n}=0.\end{aligned} \tag{3}$$

Here $\kappa'=2M'/L$ is the broadside (which we take here to mean exactly transverse) coupling coefficient between the lines.

More generally, many lines may be coupled together. For example, Fig. 1(c) shows a semi-infinite MI waveguide array, centrally fed by a single line. Within the array, (*m*, *n*) denotes the n^{th} element in the m^{th} line, *m* ranges from minus to plus infinity, and *n* ranges from 0 to infinity. The m^{th} line is again coupled to its neighbors, the $m-1^{th}$ and $m+1^{th}$ lines, via mutual inductances *M′*. If the coupling coefficients are as before, the governing equation for element (*m*, *n*) is:

$$\begin{aligned}(1-\omega_0^2/\omega^2)I_{m,n}+(\kappa/2)(I_{m,n-1}\\ +I_{m,n+1})+(\kappa'/2)(I_{m-1,n}+I_{m+1,n})=0.\end{aligned} \tag{4}$$

For a finite array, the number of equations is simply reduced, and the equations at the edge of the array are modified to omit coupling to absent neighbors. Equation (4) can, of course, be solved in full. For example, simple re-arrangement gives:

$$\begin{aligned}I_{m,n+1}=-(2/\kappa)\{(1-\omega_0^2/\omega^2)I_{m,n}+(\kappa/2)I_{m,n-1}\\ +(\kappa'/2)(I_{m-1,n}+I_{m+1,n})\}.\end{aligned} \tag{5}$$

Ignoring reflections, Eq. (5) allows solutions to be found by iteration. For example, Fig. 2(a) shows results obtained using

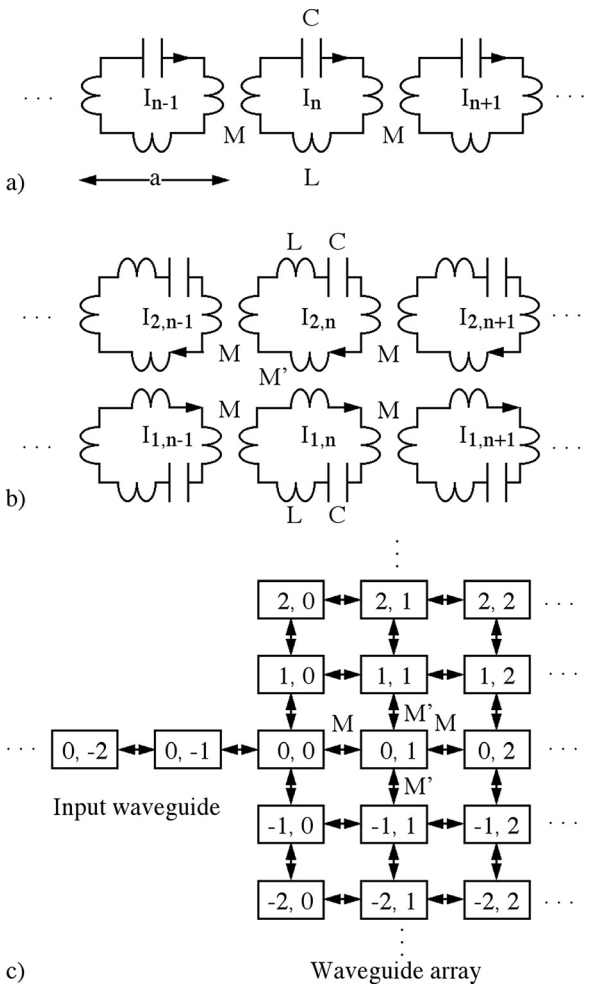

FIG. 1. (a) Magneto-inductive waveguide; (b) directional coupler; (c) centrally excited coupled waveguide array.

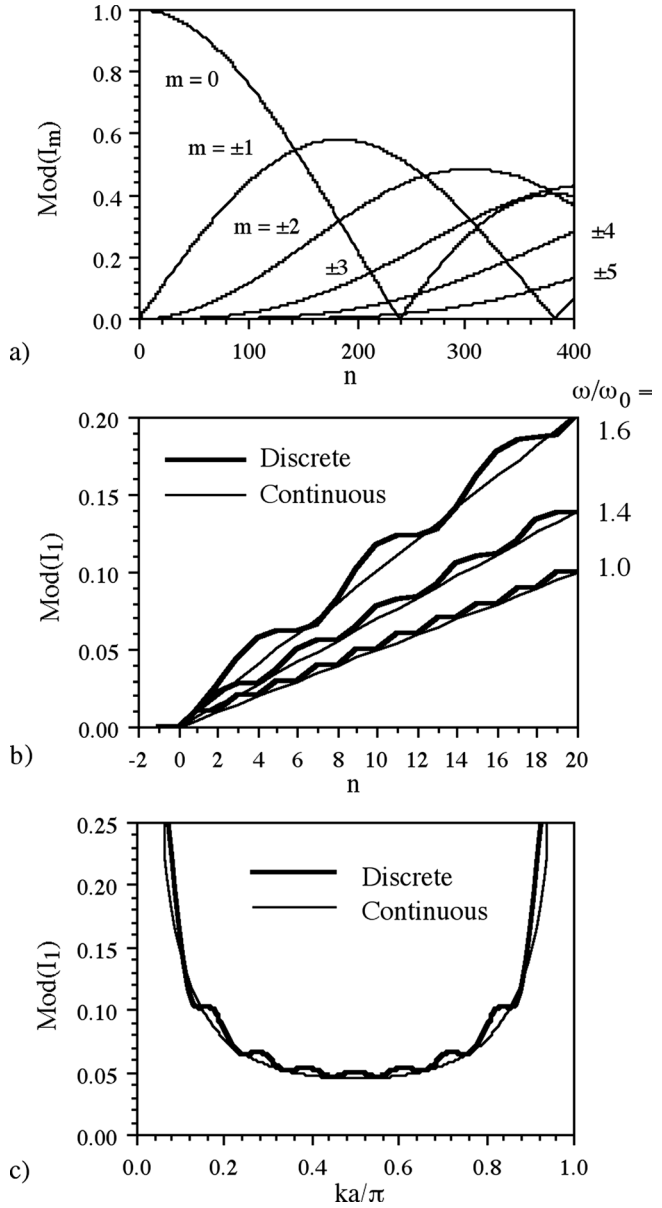

FIG. 2. (a) Numerical solution of Eq. (5), for an array of coupled MI waveguides with $\kappa = 0.7$, $\kappa' = -0.007$, $\omega/\omega_0 = 1$, and varying n. The lines show current moduli for guides near guide 0, which is excited by a wave of unit amplitude. (b) Approximate variation of cross-coupled current with n, for small n and different values of ω/ω_0; (c) corresponding variation with ka, for a nine-element line. In each case $\kappa = 0.7$ and $\kappa' = -0.007$. Thin lines show the prediction of the continuous model, thick lines show the discrete model.

the typical coupling coefficients $\kappa = 0.7$ and $\kappa' = -0.007$, and $\omega/\omega_0 = 1$, assuming the boundary conditions for $n < 0$ of $I_{0,n} = \exp(-jnka)$ and $I_{m,n} = 0$ for $m \neq 0$ in an array containing 21 lines. These conditions correspond to excitation by a current wave of unit amplitude in line 0. Here the results are plotted as current moduli, for $n \geq 0$. Initially, the current in line 0 is unity, while the current in all other lines is zero. However, the lines gradually exchange power, and lines further from the input are excited as the signals propagate. Large cross-talk may therefore arise if lines run parallel for sufficient distance. However, the distances here (determined by the value of n) are very large.

C. Power conservation and nonnearest neighbor effects

Note that, as presented, Eq. (5) will not yield a solution that conserves power. In general, the inclusion of reflected waves is required; for a full treatment for a two-line system, see Ref. 15. However, for weakly coupled systems, power is approximately conserved. The model also neglects nonnearest neighbor transverse coupling, which will provide a mechanism for a more rapid growth of cross-talk. However, additional terms may easily be included in the equations to describe such effects.

III. CROSS-TALK ESTIMATION

We now consider some analytic solutions relevant to cross-talk estimation. We use two approaches: weakly coupled continuous and discrete models.

A. Continuous model

We first return to the governing equation for a semi-infinite MI waveguide array. Figure 2(a) has shown that current amplitudes change slowly with distance if the broadside coupling is weak. We therefore assume solutions for the individual currents in an array in the form of traveling waves with slowly-varying amplitudes, as $I_{m,n} = i_{m,n} \exp(-jnka)$ where $i_{m,n}$ is the wave amplitude. With this assumption, Eq. (4) becomes:

$$(1 - \omega_0^2/\omega^2) i_{m,n} + (\kappa/2)\{i_{m,n-1} \exp(+jka) + i_{m,n+1} \exp(-jka)\} + (\kappa'/2)(i_{m-1,n} + i_{m+1,n}) = 0. \quad (6)$$

Using the dispersion equation for a linear MI waveguide, we then get:

$$\kappa\{(i_{m,n-1} - i_{m,n}) \exp(+jka) + (i_{m,n+1} - i_{m,n}) \exp(-jka)\} + \kappa'(i_{m-1,n} + i_{m+1,n}) = 0. \quad (7)$$

If the amplitudes $i_{m,n}$ are indeed slowly varying, we can write $(i_{m,n} - i_{m,n-1}) \approx (i_{m,n+1} - i_{m,n})$ and Eq. (7) reduces to:

$$(i_{m,n+1} - i_{m,n}) + j\{\kappa'/2\kappa \sin(ka)\}(i_{m-1,n} + i_{m+1,n}) = 0. \quad (8)$$

Approximating the discrete amplitude $i_{m,n}$ by a continuous function $i_m(z)$, where $z = na$, and assuming that $di_m/dz \approx (i_{m,n+1} - i_{m,n})/a$ we then get:

$$di_m/dz + j\kappa'_{\text{eff}}(i_{m-1} + i_{m+1}) = 0. \quad (9)$$

Where $\kappa'_{\text{eff}} = \kappa'/\{2\kappa a \sin(ka)\}$ is an effective transverse coupling coefficient. Equation 9 is the recurrence formula for Bessel functions, and is well known from the theory of coupled optical waveguide arrays.[47] Assuming the boundary conditions on $z = 0$ of $i_0 = 1$, $i_m = 0$ for $m \neq 0$, it has the solution:

$$i_m(z) = (-j)^m J_m(2\kappa'_{\text{eff}} z). \quad (10)$$

Here, J_m is the m^{th} order Bessel function of the first kind. These variations can be shown to agree almost exactly with the results of Fig. 2(a).

When the coupling length $\kappa'_{\text{eff}}z$ is small [i.e., near the left-hand end of Fig. 2(a)], the solutions may be approximated as:

$$i_0 \approx 1; i_{-1} = i_{+1} \approx -j\kappa'_{\text{eff}}z, \quad i_{\pm m} \approx 0 \text{ for } m > 1. \tag{11}$$

These solutions correspond to linearly increasing wave amplitudes in the two guides on either side of the input guide, which carries an undepleted wave. In this regime, cross-talk increases linearly with distance. The rate is determined by κ'_{eff}, which has a minimum of $\kappa'/2\kappa a$ when $ka = \pi/2$ and rises to infinity when $ka = 0$ or π. Consequently, cross-talk will be very high at the band edges. However, this feature is of limited practical concern, since operation will almost certainly take place near mid-band.

To illustrate this approximate solution, the thin lines in Fig. 2(b) show the variation of $|i_1|$ with n, calculated using Eq. (11) for the previous parameters ($\kappa = +0.7, \kappa' = -0.007$) and different values of ω/ω_0. In each case, the variation is linear. Similarly, the thin line in Fig. 2(c) shows the variation with ka of $|i_1|$ for a 9-element line with the same coupling coefficients. For $a = 100$ mm, this value of n corresponds to a 1 m cable. The variation is symmetric about $ka = \pi/2$ and approximately parabolic.

B. Discrete model

To see the effect of the discrete nature of MI waveguides, we now develop an alternative model. We again focus on the regime in which the input wave is hardly depleted, and only the waves in the adjacent guides are significant. Assuming that the wave in line 0 is now fixed at $I_{0,n} = \exp(-jnka)$, the equations we must solve for the currents in guides -1 and $+1$ are identical, so we consider only the latter. The relevant equation from Eq. (4) is then:

$$(1 - \omega_0^2/\omega^2)I_{1,n} + (\kappa/2)\{I_{1,n-1} + I_{1,n+1}\} = -(\kappa'/2)\exp(-jnka). \tag{12}$$

To find a solution, we adopt the approach used for inhomogeneous differential equations, which involves a particular integral (PI) and a complementary function (CF). We first identify the PI. Previous results suggest the linearly varying solution $I_{1,n} = I_1 n \exp(-jnka)$. Substitution yields:

$$(1 - \omega_0^2/\omega^2)I_1 n \ \exp(-jnka) + (\kappa/2)\{(n-1)\exp(+jka) + (n+1)\exp(-jka)\}(I_1) \ \exp(-jnka) = -(\kappa'/2) \ \exp(-jnka). \tag{13}$$

Using the dispersion equation, this relation can be simplified to:

$$(\kappa/2)\{-\exp(+jka) + \exp(-jka)\}I_1 \exp(-jnka) = -(\kappa'/2)\exp(-jnka). \tag{14}$$

And hence the cross-coupled current amplitude must be:

$$I_1 = -j\{\kappa'/[2\kappa \sin(ka)]\}. \tag{15}$$

The overall current amplitude variation $I_1 n$ clearly corresponds to the linear amplitude variation i_1 found using the continuous model. However the solution does not satisfy the boundary conditions ($I_{1,n} = 0$ for $n = 0$ and $n = -1$). To do so, we require CF terms. The LHS of Eq. (12) suggests that these must be forward- and backward-traveling waves, so the complete solution is $I_{1,n} = I_1 n \ \exp(-jnka) + I_1' \exp(-jnka) + I_1'' \ \exp(+jnka)$, where I_1' and I_1'' are unknown coefficients. Invoking the boundary condition at $n = 0$ we obtain $I_1'' = -I'$. Similarly, using the condition at $n = -1$, we obtain $I_1' = -j\, I_1 \exp(jka)/[2 \sin(ka)]$. The full solution is therefore:

$$I_{1,n} = -j\{\kappa'/[2\kappa \sin(ka)]\}\{n\exp(-jnka) - [\sin(nka)/\sin(ka)]\exp(jka)\}. \tag{16}$$

The thick lines in Figs. 2(b) and 2(c) show typical variations of the cross-coupled current $I_{1,n}$ with n and ka respectively, using the same parameters as before. In each case, the discrete solution is similar to the continuous one, but there is now additional fine structure imposed on the previously smooth variations. The discrete model can be shown to agree exactly with the prediction of the iterative method, Eq. (5).

We can use these results to impose conditions on the design of MI waveguide arrays. At mid-band, both models suggest that the cross-talk is $|I_{2,n}| \approx |n\kappa'/2\kappa|$. If we require the cross-talk to be below a given maximum (say, $|I_{2,n}| < \alpha$) after propagating N elements, the coupling coefficient must satisfy:

$$|\kappa'/\kappa| < (2\alpha/N). \tag{17}$$

For example, to reduce cross-talk below -20 dB ($\alpha = 0.1$) in a 9-element line, we require $|\kappa'/\kappa| < 0.022$, while to reach -40 dB we require $|\kappa'/\kappa| < 0.0022$. Low cross-talk will therefore only be obtained if the coupling between lines can be made very weak.

IV. MAGNETO-INDUCTIVE CABLES

We now consider magneto-inductive cable, a high-performance variant of MI waveguide formed on a flexible substrate.

A. Physical arrangement

Each resonant element consists of pairs of inductor loops and capacitor plates formed by patterning conductive layers on either side of a thin dielectric layer. Figure 3(a) shows the arrangement and Fig. 3(b) the equivalent circuit of a unit cell. If the two inductors each have inductance $L/2$ and the two capacitors have capacitance $2C$, the unit cell is equivalent to that of a conventional MI waveguide. Figure 3(c) shows the formation of a cable by overlaying unit cells on either side of the substrate. Here, alternate elements have been displaced slightly for clarity. The nearest neighbor coupling coefficient is derived from mutual inductance in the shaded areas. Its maximum possible value is now limited to $+1$. Values close to this are obtained

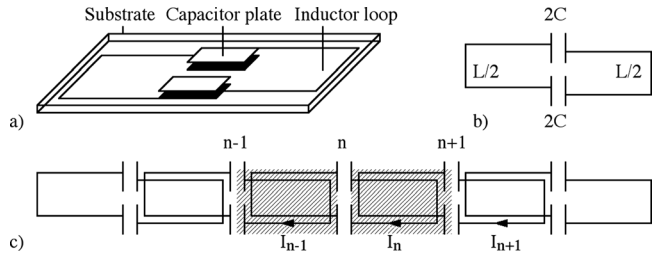

FIG. 3. Magneto-inductive cable: (a) arrangement and (b) unit cell; (c) periodic line.

experimentally, and second nearest neighbor coefficients are extremely small.

B. Numerical estimation of parameters

Detailed estimates of parameters may be obtained as follows. The resonant elements are typically long rectangular loops, as shown in Fig. 4(a). Ignoring the capacitors (which are small), the inductors are rectangles of length $2a$ and width b formed using rectangular tracks of width w and thickness t. Assuming (for example) $a=100$ mm, $b=5$ mm, $w=0.5$ mm, and $t=35$ μm, numerical simulation using the multipole-accelerated 3D inductance extraction program FastHenry[49] yields a self-inductance of $L=3.03\times10^{-7}$ H.

Coupling between adjacent elements in the same line may then be estimated using the geometry in Fig. 4(b). Here, two inductors with a small separation corresponding to the substrate thickness are overlaid with a longitudinal offset d. Similarly, coupling between elements in arrangements such as the cable arrays considered in Sec. 5 may be estimated using the geometry in Fig. 4(c), which shows two inductors with an additional transverse offset p. The full lines in Fig. 5(a) show numerically calculated variations of the coupling coefficient $\kappa=2M/L$ with longitudinal offset d, calculated for the parameters above but assuming different values of p. For $p=0$, the coupling coefficient varies quasilinearly with $|d|$, and decreases from a maximum close to $+2$ when $d=0$ through $+1$ when $|d|=a$ almost exactly to zero when $|d|=2a$. The dashed lines show idealized variations for $p=0$ and $p=b$. The nearest neighbor longitudinal coupling coefficient is almost exactly unity, while second neighbor coupling is negligible.

When $p=b$ or $p=2b$ there is a significant transverse offset between the elements. The coupling coefficient is now negative, and has a significantly reduced magnitude, but still

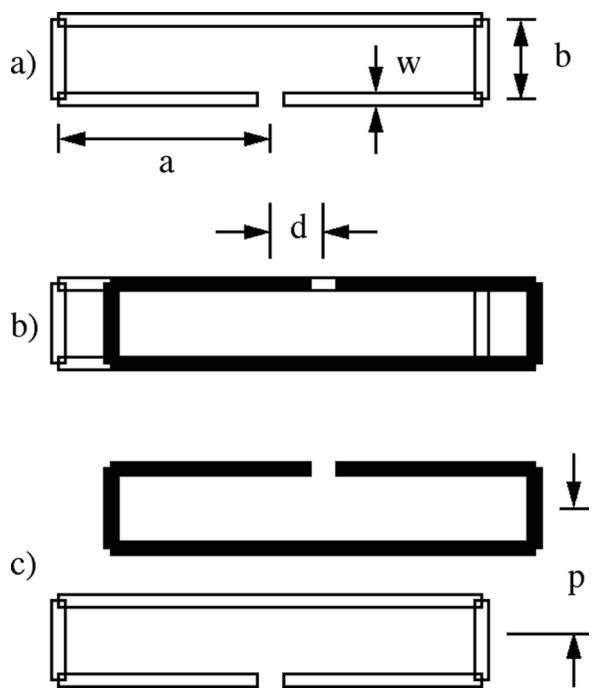

FIG. 4. (a) Single inductor, (b) longitudinally coupled pair, (c) broadside coupled pair.

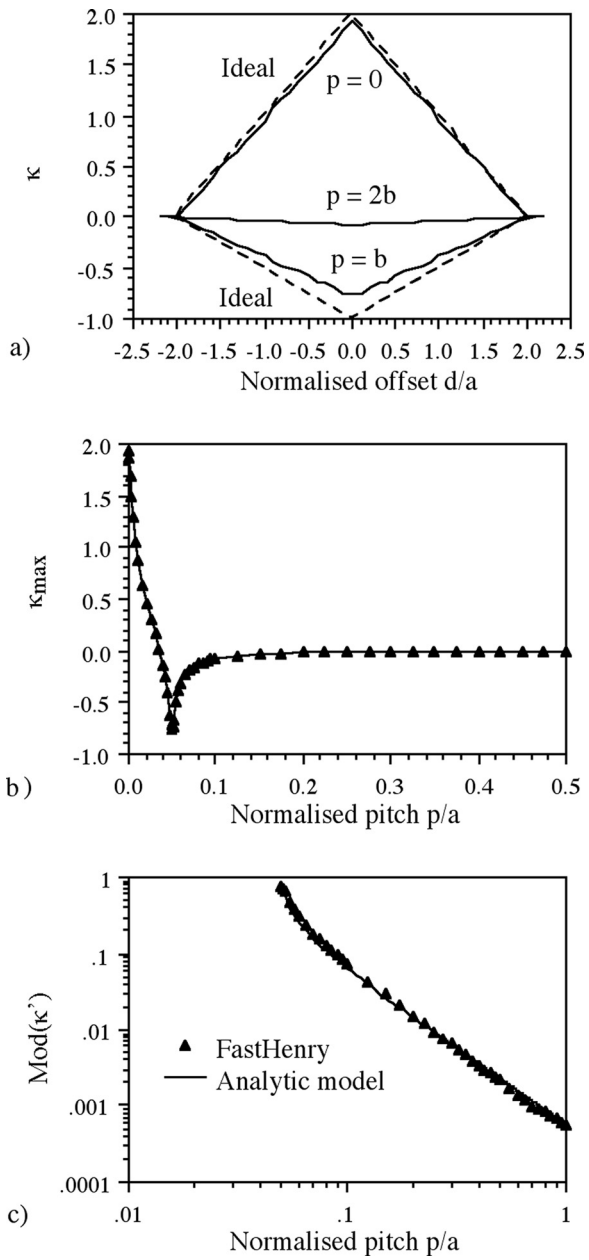

FIG. 5. (a) Numerical variation of coupling coefficient with longitudinal offset d, assuming $a=100$ mm, $b=5$ mm, $w=0.5$ mm and $t=0.0035$ mm, (b) numerical variation of broadside coupling coefficient κ_{max} with transverse offset (or pitch) p. (c) Comparison between models for the variation of broadside coupling coefficient with pitch.

varies quasilinearly with $|d|$. In general we may therefore conclude that the nearest neighbor coupling coefficient κ varies as:

$$\kappa = \kappa_{\max}(1 - |d/2a|) \text{ for } |d/a| \leq 2,$$
$$\kappa = 0 \text{ for } |d/a| > 2. \tag{18}$$

Here $\kappa_{\max}$ is the coupling coefficient when the elements are broadside on. This variation has the form of an auto-correlation between two rectangular regions of overlap.

Figure 5(b) shows the numerically calculated variation of $\kappa_{\max}$ with the normalized lateral offset or pitch p/a, for the same parameters as before. $\kappa_{\max}$ reduces from approximately $+2$ to -1 as p varies from 0 to b, passing through zero at approximately $p = 2b/3$. Similarly, for $p > b$, $\kappa_{\max}$ is negative and its value gives the broadside coupling coefficient κ' used previously. In this regime, its modulus reduces monotonically as p increases.

C. Analytic estimation of parameters

Parameters may also be estimated using a parallel-wire approximation. For example, the self-inductance of a length $2a$ of two wires of radius r separated by a distance b is:

$$L = 2a(\mu_0/\pi)\log_e\{(b-r)/r\}. \tag{19}$$

For comparison with a coil constructed using rectangular wires of width w and thickness t, we may approximate r as a geometric mean of the cross-sectional dimensions, as $r = \sqrt{(wt)}/2$. For the parameters above, we obtain $L = 3.5 \times 10^{-7}$ H, close to the earlier numerical result. Similarly, when p is sufficiently large that the inductors no longer overlap, the mutual inductance obtained broadside on may be estimated as:

$$M' = 2a(\mu_0/2\pi)\log_e\{(p^2 - (b-r)^2)/(p^2 - r^2)\}. \tag{20}$$

Consequently, κ' may be estimated as:

$$\kappa' = \log_e\{(p^2 - (b-r)^2)/(p^2 - r^2)\}/\log_e\{(b-r)/r\} \quad \text{for } p > b. \tag{21}$$

Figure 5(c) compares numerical and analytic results for the variation of κ' with p, for the same elements as before. The agreement is excellent. Both models show that κ' decays approximately as p^{-2}, implying that doubling the pitch in an array will reduce broadside coupling coefficients and coupled amplitudes fourfold, and hence reducing coupled powers by a factor of 16 (or 12 dB). The same argument implies that cross-talk in nonnearest neighbor guides will be 12 dB below that in nearest neighbors.

V. MAGNETO-INDUCTIVE CABLE ARRAYS

Cable arrays are formed by placing cables side-by-side with a pitch p as shown in Fig. 6(a). Because of the overlap of elements in the same line, the coupling between lines will be more complicated and in this section we describe the resulting effects.

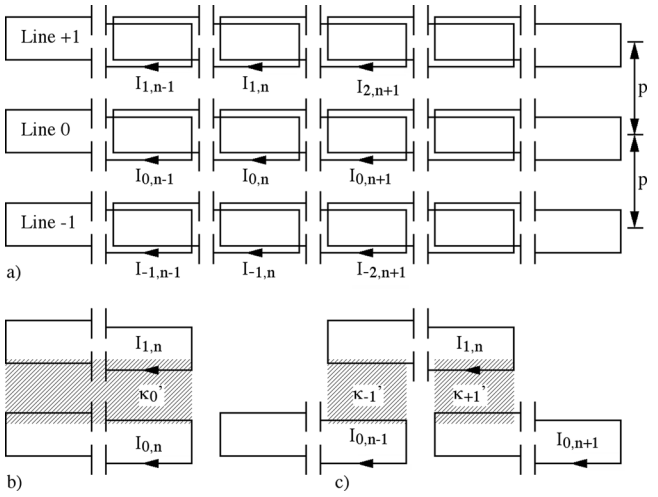

FIG. 6. MI cable array: (a) arrangement; (b) and (c) origin of cross-coupling coefficients.

A. Effect of cable coupling

The main effect of coupling will be additional coupling terms. The coefficients may be estimated much as before. Clearly, there will be a coupling coefficient κ_0' between corresponding elements $(1, n)$ and $(0, n)$ in each line, as shown by the shaded overlap region in Fig. 6(b). The value of this term will be the broadside coupling coefficient κ'. However, there will also be coupling κ_{-1}' between element $(1, n)$ and element $(0, n-1)$ and κ_{+1}' between elements $(1, n)$ and $(0, n+1)$ as shown in Fig. 6(c). Using the results of Sec. 4, these terms can be estimated as $\kappa_{-1}' = \kappa_{+1}' \approx \kappa'/2$.

Thus, for coupled cables, the circuit equations for lines 0 and 1 have the modified form:

$$\begin{aligned}(1-\omega_0^2/\omega^2)I_{1,n} + (\kappa/2)\{I_{1,n-1} + I_{1,n+1}\} \\ + (\kappa'/2)\{I_{0,n-1}/2 + I_{0,n} + I_{0,n+1}/2\} = 0. \\ (1-\omega_0^2/\omega^2)I_{0,n} + (\kappa/2)\{I_{0,n-1} + I_{0,n+1}\} \\ + (\kappa'/2)\{I_{1,n-1}/2 + I_{1,n} + I_{1,n+1}/2\} = 0.\end{aligned} \tag{22}$$

Here, we have ignored coupling to any other lines. In the weak coupling regime, the equation that must be solved for line 1 is then:

$$\begin{aligned}(1-\omega_0^2/\omega^2)I_{1,n} + (\kappa/2)\{I_{1,n-1} + I_{1,n+1}\} \\ = -(\kappa'/2)\{\exp(+jka)/2 + 1 + \exp(jka)/2\}\exp(-jnka).\end{aligned} \tag{23}$$

Or alternatively:

$$(1-\omega_0^2/\omega^2)I_{1,n} + (\kappa/2)\{I_{1,n-1} + I_{1,n+1}\} = -(\kappa'/2) \times\{1 + cos(ka)\}\exp(-jnka)\}. \tag{24}$$

Clearly, the effect of the additional coupling terms in a cable is to alter the transverse coupling coefficient between the lines to a new value of $\kappa'_{\text{cable}} = \kappa'\{1 + \cos(ka)\}$. Since κ'_{cable} is now dependent on ka, we would expect changes in the frequency dependence of the solution. For example, when $ka = \pi$, there can be no net coupling, since $\cos(ka) = -1$. In this case, the additional coupling terms

lead to cross-coupled currents that cancel the main current induced by broadside coupling. However, when $ka = 0$ there will be increased coupling, since the additional terms lead to in-phase cross-coupled currents.

B. Modified cross-talk variation

By inspection, the discrete model then gives for the current $I_{1,n}$:

$$I_{1,n} = -j\{\kappa'_{\text{cable}}/[2\kappa \sin(ka)]\}\{n\exp(-jnka) - [\sin(nka)/\sin(ka)]\exp(jka)\}. \quad (25)$$

The effect of cable-type coupling is then to alter the frequency dependence of any cross-talk. Figure 7 shows the variation of the cross-coupled power $P_1 = |I_1|^2$ (in dB) with ω/ω_0, for a 9-element line with the previous parameters ($\kappa = 0.7$ and $\kappa' = -0.007$). The results obtained with simple broadside coupling are superimposed for comparison. The curves intersect when $\omega/\omega_0 = 1$. However, cable coupling makes the response highly asymmetric, with somewhat increased cross-talk when $\omega/\omega_0 < 1$ and much reduced cross-talk when $\omega/\omega_0 > 1$. Strategies to reduce cross-talk are clearly important and will be considered in Sec. 7.

VI. EXPERIMENTAL RESULTS

We now investigate the validity of the theoretical model using experiments carried out on thin-film MI cable fabricated by double-sided patterning of copper-clad polyimide.

A. Experimental configuration

The starting material was 25 μm thick Kapton® HN (DuPont, Circleville, OH), coated on each side with a 35 μm thick pressure-bonded layer of copper and patterned by lithography and wet etching. Cables were fabricated in 2 m lengths containing 24 parallel lines. In each case, the element length and width were $2a = 200$ mm, and $b = 4.7$ mm respectively, and the track width was $w = 0.5$ mm, but other parameters were varied across the array. From these variants, cables with particular properties (established using separate experiments detailed in Ref. 47) were selected.

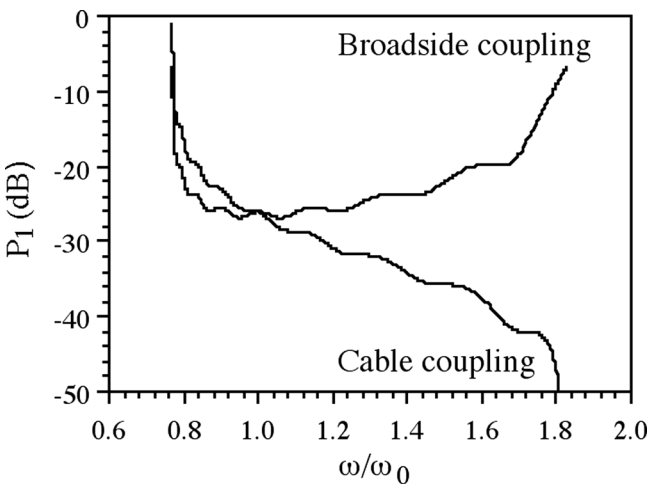

FIG. 7. Variation of cross-coupled power with normalized frequency, for a nine-element magneto-inductive cable with $\kappa = 0.7$ and $\kappa' = -0.007$. Also shown for comparison are the corresponding results obtained with simple broadside coupling.

The cables used had inductor and capacitor lengths of 90 mm and 10 mm respectively, giving an inductance of $L = 240$ nH and a capacitance of $C = 10$ pF. The resonant frequency $f_0 = \omega_0/2\pi$ was then approximately 100 MHz, and the Q factor at this frequency was 48. The mutual inductance was $M = 81$ nH, so that the longitudinal coupling coefficient was $\kappa = 0.675$ and the mid-band impedance was $Z_{0M} = 48.6\ \Omega$. Because Z_{0M} was close to 50 Ω impedance, it was simple to carry experiments with properly terminated guides. Each guide was therefore equipped with input and output transducers, consisting of single inductors $L/2$ made resonant at the element resonant frequency ω_0 using single capacitors $2C$. Elsewhere,[49] it has been shown that such transducers provide an excellent match to resistive loads over most of the propagating band and hence largely suppress end-reflections. Measurements were made with an electronic network analyser (ENA) with 50 Ω characteristic impedance (Agilent E5061A).

For cross-talk investigations, cables were separated, shortened to 1 m lengths (which contained nine resonant elements and two transducers) and mounted on straight wooden formers to allow cables to run parallel with arbitrary separation. Figure 8(a) shows a photograph of two neighboring cables. The properties of isolated cables were first established by connecting input and output to the ENA. Figure 9(a) shows the frequency variation of the S-parameters. The variation of S_{21} shows bandpass propagation, ranging from ≈70 MHz to ≈160 MHz, with a minimum insertion loss of ≈3 dB at ≈100 MHz. The cutoff is slower at high frequencies, presumably because of loss. The variation of S_{11} shows reflection below −15 dB over the majority of the propagating band, suggesting that the coupling transducers are effective. However, reflections rise rapidly at the band edges, implying ineffective excitation at these frequencies.

The properties of coupled cables were investigated by connecting the input of one cable (Cable 0) to the S_{11} port of the ENA and the output of the other (Cable 1) to the S_{21} port, terminating unused cable ends with 50 Ω loads as

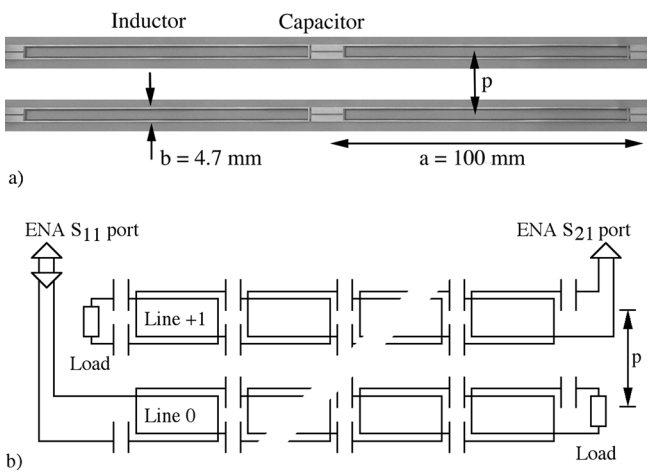

FIG. 8. (a) Photograph of and (b) arrangement for testing coupled magneto-inductive cable.

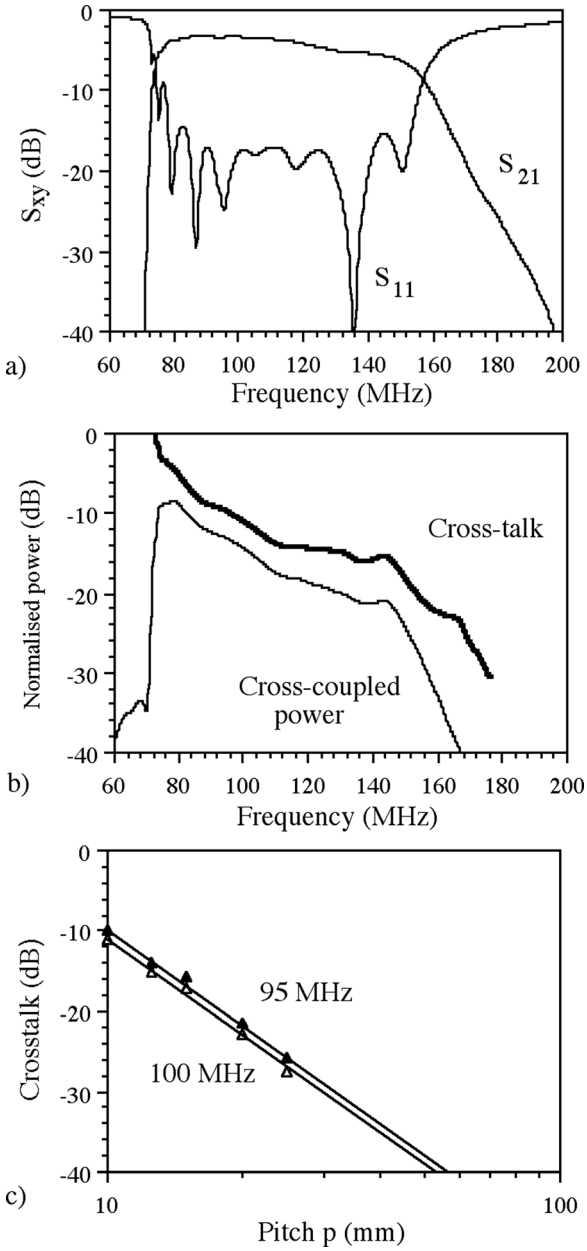

FIG. 9. Frequency-variation of (a) S-parameters, for single cable, and (b) cross-coupled power and normalized cross-talk between paired cables; (c) variation of cross-talk with pitch p.

shown in Fig. 8(b). Figure 9(b) shows the frequency variation of cross-coupled power thus obtained. Here, a small separation ($p = 10$ mm) was used deliberately, to cause strong cross-talk. The variation is again band-limited, but the cross-coupled power is considerably reduced at high frequency compared with Fig. 9(a). Figure 9(b) also shows the cross-talk variation after correction for the excitation efficiency. This data generally follows the asymmetric variation shown in Fig. 7, with cross-talk increasing at low frequency and reducing at high. Similar results were obtained at larger separations p, with overall cross-talk reducing as p increased. The data points in Fig. 9(c) show the variation of cross-talk with cable pitch, at 95 and 100 MHz frequency. The lines show a theoretical fit, assuming the coupling coefficients falloff as p^{-2} as estimated earlier. There is clearly good agreement with the simple model.

VII. CROSS-TALK REDUCTION

The relatively slow decay of cross-talk with pitch suggests that additional efforts should be used to minimize interaction between lines in dense MI cable arrays. For coupled optical waveguide arrays, coupling is typically reduced by dephasing (i.e., by varying the propagation constant between guides).[46] If this is done, contributions coupled from guide to guide no longer add together in-phase. For MI cables, all that is required is to vary the angular resonant frequency ω_0 of the elements from line to line, ideally keeping $\omega_0 M$ constant in the process so that impedance matching may be maintained. However, for MI waveguides, the ability to define elements of essentially arbitrary shape allows additional possibilities to reduce the coupling coefficients between neighboring guides by cancellation of induced currents.

For example, Fig. 10(a) shows a modified resonant element, in which the capacitor positions have been altered and the right-hand inductor has been twisted twice. With the capacitors placed as shown, the structure can still be formed using patterned conducting layers on either side of a thin substrate. Figure 10(b) shows a simplified version of this element, omitting the capacitors but showing the sense of current flow in each part of the resonant loop. Figure 10(c) shows how a single line may be formed by overlaying elements whose orientations are repetitively reflected. Alternate elements are again slightly displaced, for clarity. This arrangement is difficult to construct on a single substrate, but relatively simple to form by stacking together two substrates carrying alternate elements. Finally, Fig. 10(d) shows how a cable pair may be constructed from adjacent lines that are staggered so that alternating sections of each element abut.

Figure 10(e) shows the overlap that contributes to the transverse coupling coefficient κ_0', while Fig. 10(f) shows

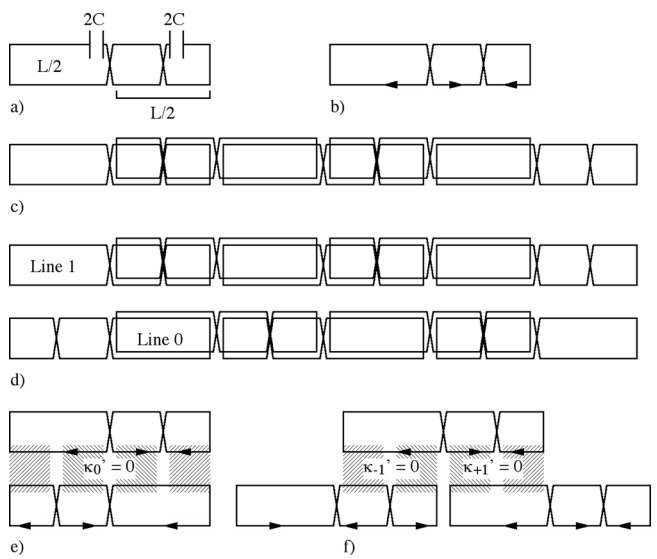

FIG. 10. a) Twisted element, b) simplified element, c) and d) single line and coupled lines formed from twisted elements, e) and f) origin of nearest-neighbour cross-coupling terms.

the corresponding contributions to κ_{-1}' and κ_{+1}'. In each case the sign of the contribution can be determined from the direction of current flow, and is indicated by the slope of the crosshatched lines. For all three terms, the distribution of current flow suggests that the induced currents will have different signs in different regions. As a result, cancellation of induced currents may occur. With careful design, the net coupling coefficient will be approximately zero, so that all three contributions to cable coupling can be largely eliminated. Although there is no corresponding reduction in second nearest neighbor effects, this example suggests that considerable reduction in nearest neighbor cross-talk might well be possible.

VIII. CONCLUSIONS

The behavior of parallel arrays of identical magneto-inductive waveguides has been investigated, using both discrete and continuous models. Simple theoretical methods for estimating cross-talk have been developed for arrays containing simple MI waveguides, and for the slightly different case of MI cable arrays, and the theory has been broadly verified using experiments carried out with thin-film cable. The main factors affecting cross coupling have been identified, and a strong frequency-dependence of the cross-talk (the exact variation of which depends on the cable configuration) has been predicted and observed. Suggestions for cross-talk reduction by cancellation of induced currents using improved element layouts have been made. Future work will focus on development of practical low cross-talk systems.

We have focused on magnetic coupling, rather than electric coupling. We may illustrate the relative significance of the latter by comparing the capacitance of the parallel-plate components contained in the resonant elements with other mutual capacitances. Clearly, there are several terms that might be considered; here we restrict ourselves to broadside coupling between the closest coplanar plates of nearest neighbors.

The per-unit-length capacitance C_P of a parallel plate capacitor of width w_C, dielectric thickness t_S, and relative dielectric constant ε_r is $C_P = \varepsilon_0 \varepsilon_r w_C / t_S$, where ε_0 is the dielectric constant of free space. For the flexible MI cable, $w_C \approx b/2$, so $w_C \approx 2.5$ mm for $b = 5$ mm. Assuming a polyimide substrate ($\varepsilon_r = 3.5$) of thickness $t_S = 25$ μm, we obtain $C_P \approx 3500$ ε_0 F/m. Similarly, the per-unit-length capacitance C_P' between coplanar plates of the same width separated by a distance s can be found from coplanar waveguide theory[50] as $C_P' = \varepsilon_0 K'(k)/K(k)$, where $K(k)$ is a complete elliptic integral of the first kind, $K'(k) = K(k')$, $k^2 = 1 - k'^2$ and $k = s/(s + 2w_C)$. Assuming a pitch p, the separation between the corresponding plates of capacitors from adjacent neighbors is $s = p - 2w_C$, so that $k \approx (p - b)/p$. The minimum realistic separation is $p - b \approx 1$ mm, so the minimum likely value of k is around 1/6. At this value, $K'(k)/K(k) \approx 2$, so $C_P' \approx 2\varepsilon_0$ F/m. In the worst case, we would therefore expect C_P' still to be at least a thousand times smaller than C_P. In contrast, the values of M'/L considered here have been much larger, in the range $0.1 < |M'/L| < 0.5$ for small separations. Electric coupling effects are therefore likely to be relatively small. However, this may not be the case in equivalent structures based on split-ring resonators, where the element capacitance itself arises from a coplanar geometry, and hence is much smaller.

[1] E. Shamonina, V. A. Kalinin, K. H. Ringhofer, and L. Solymar, Electron Lett. **38**, 371 (2002).
[2] M. C. K. Wiltshire, E. Shamonina, I. R. Young, and L. Solymar, Elect. Lett. **39**, 215 (2003).
[3] E. Shamonina and L. Solymar, J. Phys. D Appl. Phys. **37**, 362 (2004).
[4] E. Shamonina, V. A. Kalinin, K. H. Ringhofer, and L. Solymar, J. Appl. Phys. **92**, 6252 (2002).
[5] R. R. A. Syms, E. Shamonina, and L. Solymar, Eur. Phys. J. B **46**, 301 (2005).
[6] O. Zhuromskyy, E. Shamonina, and L. Solymar, Proc. SPIE **5955**, 1 (2005).
[7] A. Radkovskaya, M. Shamonin, C. J. Stevens, G. Faulkner, D. J. Edwards, E. Shamonina, and L. Solymar, J. Magn. Magn. Mater. **300**, 29 (2006).
[8] R. R. A. Syms, E. Shamonina, V.Kalinin, and L. Solymar, J. Appl. Phys. **97**, 064909 (2005).
[9] R. R. A. Syms, I. R. Young, and L. Solymar, J. Phys. D. Appl. Phys. **39**, 3945 (2006).
[10] R. R. A. Syms, O. Sydoruk, E. Shamonina, and L. Solymar, Metamaterials **1**, 44 (2007).
[11] O. Sydoruk, O. Zhuromskyy, E. Shamonina, and L. Solymar, Appl. Phys. Lett. **87**, 072501 (2005).
[12] A. Radkovskaya, O. Sydoruk, M. Shamonin, E. Shamonina, C. J. Stevens, G. Faulkner, D. J. Edwards, and L. Solymar, IET Proc. Microwaves, Antennas Propag. **1**, 80 (2007).
[13] M. J. Freire, R. Marques, F. Medina, M. A. G. Laso, and F. Martin, Appl. Phys. Letts. **85**, 4439 (2004).
[14] I. S. Nefedov and S. A. Tretyakov, Micr. Opt. Tech. Lett. **145**, 98 (2005).
[15] R. R. A. Syms, E. Shamonina, and L. Solymar, IEE Proc. Microwaves, Antennas Propag. **153**, 111 (2006).
[16] A. Radkovskaya, O. Sydoruk, M. Shamonin, C. J. Stevens, G. Faulkner, D. J. Edwards, E. Shamonina, and L. Solymar, Microwave Opt. Technol. Lett. **49**, 1054 (2007).
[17] M. C. K. Wiltshire, E. Shamonina, I. R. Young, and L. Solymar, Progress in Electromagnetics Research Symposium, Honolulu, Hawaii, USA 13–16 October 2003.
[18] M. C. K. Wiltshire, E. Shamonina, L. Solymar, and I. R. Young, Proceedings of the Annual Meeting of the International Society for Magnetic Resonance in Medicine (ISMRM 11), p 1582, Toronto, Ontario, Canada 10–16 July 2004
[19] M. J. Freire and R. Marques, Appl. Phys. Lett. **86**, 182505 (2005).
[20] M. J. Freire and R. Marques, J. Appl. Phys. **100**, 063105 (2006).
[21] M. J. Freire, R. Marques, and L. Jelinek, Appl. Phys. Lett. **93**, 231108 (2008).
[22] O. Sydoruk, M. Shamonin, A.Radkovskaya, O. Zhuromskyy, E. Shamonona, R. Trautner, C. J. Stevens, G. Faulkner, D. J. Edwards, and L. Solymar, J. Appl. Phys. **101**, 073903 (2007).
[23] L. Solymar, O. Zhuromskyy, O. Sydoruk, E. Shamonina, I. R. Young, and R. R. A. Syms, J. Appl. Phys. **99**, 123908 (2006).
[24] R. R. A. Syms, T. Floume, I. R. Young, L. Solymar, and M. Rea, Metamaterials **4**, 1 (2010).
[25] R. R. A. Syms, L. Solymar, and I. R. Young, IEEE J. Sel. Top. Quantum Electron. **16**, 433 (2010).
[26] C. J. Stevens, C. W. T. Chan, K. Stamatis, and D. J. Edwards, IEEE Trans. Microwave Theory Tech. **58**, 1248 (2010).
[27] O. Sydoruk, E. Shamonina, and L. Solymar, J. Phys. D: Appl. Phys. **40**, 6879 (2007).
[28] R. R. A. Syms, I. R. Young, and L. Solymar, Metamaterials **2**, 122 (2008).
[29] T. Floume, R. R. A. Syms, L. Solymar, and I. R. Young, Proceedings of the 3rd International Congress on Advanced Electromagnetic Materials in Microwaves and Optics, pp 132–134, London, UK 30 August–4 September 2009.
[30] J.-S. Hong and M. J. Lancaster, IEEE Trans. Microwave Theory Tech. **44**, 2099 (1996).
[31] J.-S. Hong and M. J. Lancaster, IEEE Trans. Microwave Theory Tech. **45**, 2358 (1997).
[32] S. Maslovski, P. Ikonen, I. Kolmakov, and S. Tretyakov, PIER **54**, 61 (2005).
[33] L. Jylhä, S. Maslovski, and S. Tretyakov, Progress in Electromagnetics Research Symposium, Cambridge, MA, USA 26–29 March 2009.

[34]I. V. Shadrivov, A. N. Reznik, and Y. S. Kivshar, Physica B **394**, 180 (2007).
[35]M. Eleftheriou, N. Lazarides, and G. P. Tsironis, Phys. Rev. E **77**, 036608 (2008).
[36]N. Liu, S. Kaiser, and H. Giessen, Adv Mater. **20**, 4521 (2008).
[37]J. D. Baena, L. Jelinek, R. Marques, and M. Silveirinha, Phys. Rev. A **78**, 013842 (2008).
[38]M. K. C. Wiltshire, J. V. Hajnal, J. B. Pendry, D. J. Edwards, and C. J. Stevens, Opt. Express **11**, 710 (2003).
[39]M. C. K. Wiltshire, E. Shamonina, I. R. Young, and L. Solymar, J. Appl. Phys. **95**, 4488 (2004).
[40]G. Dolling, M. Wegener, A. Schädle, S. Burger, and S. Linden, Appl. Phys. Lett. **89**, 231118 (2006).
[41]M. Decker, S. Burger, S. Linden, and M. Wegener, Phys. Rev. B **80**, 193102 (2009).
[42]H. Liu, Y. M. Liu, S. M. Wang, S. N. Zhu, and X. Zhang, Phys. Status Solidi B. **246**, 1397 (2009).
[43]R. R. A. Syms, L. Solymar, I. R. Young, and T. Floume, J. Phys. D. Appl. Phys. **43**, 055102 (2010).
[44]R. R. A. Syms and L. Solymar, Metamaterials, **4**, 161 (2010).
[45]R. R. A. Syms, L. Solymar, and I. R. Young, J. Phys. D. Appl. Phys. **43**, 285003 (2010).
[46]A. Yariv, IEEE J. Quantum Electron. **9**, 919 (1973).
[47]S. Somekh, E. Garmire, A. Yariv, H. L. Garvin, and R. G. Hunsperger, Appl. Phys. Lett. **22**, 46 (1973).
[48]R. R. A. Syms, IEEE J. Quantum Electron. **23**, 525 (1987).
[49]M. Kamon, M. J. Tsuk, and J. White Proceedings of the 30th ACM/IEEE Design Automation Conference, pp 678–683, Dallas, TX, USA 14–18 June 1993.
[50]V. Fouad Hanna, Electron Lett **16**, 604 (1980).